THE ASTROPHYSICAL JOURNAL, 493:940–949, 1998 February 1

WATER MASERS IN ORION

R. A. GAUME,[1] T. L. WILSON,[2] F. J. VRBA,[3] K. J. JOHNSTON,[1] AND J. SCHMID-BURGK[2]
Received 1997 July 8; accepted 1997 September 8

ABSTRACT

Measurements of the $6_{16} \rightarrow 5_{23}$ line of H_2O at 1.3 cm in the Orion region of star formation are reported. With a spatial resolution of $\approx 0''.1$, H_2O maser emission was detected in two regions: Orion BN/KL and Orion S. The well-known masers in the BN/KL region are distributed in a 30″ by 30″ area. The "shell" masers, within the BN/KL region, are distributed in a 2″ by 0″.5 strip centered on radio source I and are offset from IRc2. The average shell maser spectrum is doubly peaked, resembling the spectrum of the $v = 1$ SiO masers. The shell masers have deconvolved sizes of 24–38 AU, slightly smaller than the synthesized beam. Newly detected H_2O masers in the Orion S region are distributed in a 15″ by 20″ area. One cluster of masers in the Orion S region is found in a thin 0″.6 strip. The velocity range of the masers in this cluster is nearly 65 km s^{-1}. We suggest that this cluster of masers is associated with the energetic source of the Orion S molecular outflow. A search in the Orion S region for associated maser emission in the ground-state OH main lines and the $9_2 \rightarrow 10_1\, A^+$ and $6_2 \rightarrow 6_1\, E$ lines of CH_3OH gave only upper limits, as did a search for centimeter-wavelength continuum.

Near-infrared images of the Orion region are presented in the J, H, and K bands. Three objects with very red near-infrared colors were detected in the Orion S region, near the H_2O masers and the previously detected millimeter-wavelength dust continuum peak. One of these objects exhibits near-infrared colors consistent with a B2 zero-age main-sequence star. Although this object may heat the northern part of the Orion S dust cloud, its luminosity and separation from the dust maximum make it unlikely that it alone heats the entire Orion S region. More likely, the primary heat source of the Orion S region is deeply embedded in dust and completely extincted in the near-infrared.

Subject headings: masers — radio lines: ISM — stars: individual (Orion BN/KL)

1. INTRODUCTION

In the 400 μm continuum map of the OMC-1 cloud by Keene, Hildebrand, & Whitcomb (1982), there are two prominent maxima. The more intense source is the northern peak. This is the Orion KL nebula, the most studied source in OMC-1 (see, e.g., Genzel & Stutzki 1989). The second peak is located about 100″ south of Orion KL. This region is often referred to as Orion South (hereafter Orion S). Many authors have concluded that the millimeter emission in Orion S is caused by hot dust (e.g., Mundy et al. 1986). Interferometer studies at millimeter wavelengths have provided an accurate position for the millimeter continuum and have shown that this source has a FWHP size of 11″ by 7″ (Mundy et al. 1986 and McMullin, Mundy, & Blake 1993).

There are many observations of quasi-thermally excited spectral lines toward the southern peak. The 6 cm H_2CO line is found in absorption over a 30″ region (Johnston et al. 1983; Mangum, Wootten, & Plambeck 1993). There is also a maximum in the inversion lines of ammonia, referred to as S6 by Batrla et al. (1983). Ziurys, Wilson, & Mauersberger (1990) found bipolar emission in lines of SiO oriented approximately N-S from this region, with a velocity full width at zero power (FWZP) of 25 km s^{-1}. In CO, there is a highly collimated outflow lobe extending 2′ to the SW from this maximum (Schmid-Burgk et al. 1990). The CO outflow has at most only a relatively small extension in the NE direction, which may indicate that the NE flow is hindered by the presence of the Trapezium. If so, the outflow source is close to the H II/H_2 interface. Observations of transitions of SiO, SO_2, CH_3OH, and HC_3N have been presented by McMullin et al. (1993) at a wavelength of 3 mm, with a resolution of 10″.

From the presence of the CO outflow, and the small sizes of the infrared sources, there must be a compact energy source. From observations with the Effelsberg 100 m telescope, there are a number of H_2O masers in Orion S. We have followed up the 100 m observations with VLA measurements. The primary goal of the VLA observations, reported here, is to determine the center of the outflow with high accuracy, and to provide new information about the exciting source and the nearby molecular regions. We have also carried out a search in Orion S for class I and class II CH_3OH masers, ground-state OH masers, centimeter-wavelength continuum, and associated near-infrared sources.

The intense H_2O masers in the BN/KL region have been well studied (see, e.g., Genzel & Stutzki 1989). Genzel et al. (1981) measured the relative proper motions of H_2O maser features in the BN/KL region using VLBI techniques (with an absolute accuracy of $\pm 0''.5$) and discussed three different types of H_2O masers in BN/KL: low velocity, high velocity, and shell. Although Genzel et al. (1981) detected many H_2O masers in the BN/KL region and reported proper motions for both low- and high-velocity H_2O maser features, they found that the shell features were not detected, probably because they were highly resolved on the VLBI baselines used in the experiments. Although the VLA observations presented here were centered on the Orion S region, intense H_2O masers in the BN/KL region (2′ N) were easily observed. In particular, we have detected and imaged the

[1] US Naval Observatory (USNO), 3450 Massachusetts Avenue, NW, Washington, DC 20392-5420.
[2] Max-Planck-Institut für Radioastronomie, Postfach 2024, D-53010 Bonn, Germany.
[3] USNO, Box 1149, Flagstaff Station, Flagstaff, AZ 86002-1149.

shell H_2O maser features within Orion BN/KL, and report their positions, velocities, and flux densities.

2. OBSERVATIONS

2.1. *VLA*

The radio wavelength observations were made in 1991 August 5 under good weather conditions with the VLA[4] A configuration, which nominally provides baseline lengths from 0.68 to 36.4 km. The total duration of the observations was 5 hr. The central pointing position for all observations was R.A. = $05^h32^m46^s.0$, decl. = $-05°26'00''$. The primary flux density calibrator was 3C 48; observations of 3C 286 were used as a consistency check. The source 0539−057 was used for phase calibration. The observations employed both the VLA continuum system with the 3.6 cm receivers and the spectral-line system with the 1.3 and 20 cm receivers. The spectral-line observations with the 1.3 cm receivers employed a single intermediate frequency (IF) mode with 64 98 kHz (=1.3 km s^{-1}) channels, right circular polarization, and on-line Hanning weighting of the line channels. Channel 32 of the 64 was set to a local standard of rest (LSR) velocity of 5 km s^{-1}. The 1.3 cm H_2O transition (22.2 GHz) and two transitions of CH_3OH ($9_2 \rightarrow 10_1\, A^+$ at 23.1 GHz and $6_2 \rightarrow 6_1\, E$ at 25.0 GHz) were observed. The 20 cm observations employed a dual IF mode with 128 6.1 kHz channels in each IF, right circular polarization, and on-line Hanning weighting of the line channels. Channel 64 of the 128 was set to an LSR velocity of 5 km s^{-1}. One IF of the system was set to the 1665 MHz transition of OH, the other to the 1667 MHz transition.

The data were calibrated and reduced in the standard manner using the Astronomical Image Processing System software package of the NRAO. The 1.3 cm spectral-line data were transformed with natural weighting of the *uv* data and a cell size 0.″03. No CH_3OH emission was detected for either transition from Orion S within an 80 km s^{-1} band centered on 5 km s^{-1} (LSR). The rms noise in a single channel map was 18 mJy beam^{-1} for the 23.1 GHz transition and 35 mJy beam^{-1} for the 25.0 GHz transition. The 20 cm spectral-line data were transformed with uniform weighting of the *uv* data and a cell size of 0.″33. OH maser emission at both the 1665 and 1667 MHz ground-state transitions was detected toward BN/KL. The BN/KL OH masers have been the subject of previous studies (see, for example, Johnston, Migenes, & Norris 1989). No OH maser emission was detected for the 1665 or 1667 MHz transitions at Orion S within a 140 km s^{-1} band centered on 5 km s^{-1} (LSR) at an rms noise level of 25 mJy beam^{-1}. The 3.6 cm continuum data were transformed with natural weighting of the *uv* data and a cell size of 0.″065. Although many of the previously detected centimeter continuum components (see Felli et al. 1993 and references therein) were detected, no continuum components were found toward Orion S at an rms noise level of 0.1 mJy beam^{-1}.

Water maser emission was detected in both the BN/KL region and the Orion S region. The data were transformed with natural weighting of the *uv* data and a cell size of 0.″03, resulting in a FWHM beam size of 0.″1 × 0.″09, p.a. = −25°. Self-calibration was performed on a channel containing a single intense maser feature. The improved complex antenna gain solutions were applied to the entire spectral-line data set. The 63 data channels were simultaneously imaged and CLEANed in three separate fields: one field of size 1024 × 1024 pixels centered 6″ E and 2.″3 N of the central pointing position, the second of size 1024 × 1024 pixels centered 17.″1 E and 92″ N of the central pointing position, and the third of size 256 × 256 pixels centered 25.″1 E and 110″ N of the central pointing position. The FWHM primary beam of the individual antennas of the VLA is ≈2′. *All* of the detected H_2O maser features in the BN/KL region of Orion are placed beyond the 50% primary beam response. The primary beam sensitivity at the positions of the detected H_2O masers in the BN/KL region ranges from 20% to only 3%. The large intensity of the H_2O masers in the BN/KL region makes detection possible even at these decreased sensitivities; however, because of diminished sensitivity, it is likely that we have failed to detect intense maser features beyond the 3% primary beam response or weaker maser features well within the BN/KL region. An algorithm that corrects for the decreased sensitivity due to the primary beam response of the VLA antennas was applied to the two fields in the BN/KL region. The rms noise level for line channels in the Orion S field, not limited by dynamic range, was ≈15 mJy beam^{-1}. The water maser features in all channels were fitted with a two-dimensional Gaussian profile. The *relative* positional accuracy among fitted maser features is estimated to be $\frac{1}{10}$ of the synthesized beamwidth. The *absolute* positional accuracy of the fitted features is ≈0.″1.

2.2. *USNO IRCAM*

Near-infrared observations of Orion were obtained using the USNO infrared camera (IRCAM) at the 1.55 m telescope located at the Flagstaff Station of the USNO. The detector is a Rockwell 256^2 HgCdTe array operating at 77 K. Observations were obtained in the *J* (1.10–1.44 μm), *H* (1.50–1.82 μm), and *K* (2.00–2.40 μm) wavelength bands. Observations obtained on 1994 November 22 were centered SE of Orion BN/KL near $05^h32^m47^s$, $-05°24'36''$. Observations in each band consisted of five dithered sets of 20 co-added images of 0.65 s duration each on the source and a set of identical integrations located ∼10′ off-source in order to determine the sky and telescope backgrounds. Both the on-source and off-source observations were dithered by ∼30″ in order to eliminate the effects of defective pixels. The point-spread function (PSF) for each band was ≈1.″3.

Based on a series of preliminary observations obtained on 1996 January 5, much deeper *J*-, *H*-, and *K*-band observations were obtained on 1996 January 8 of an area centered south of the Orion S region near $05^h32^m46^s$, $-05°26'10''$. The PSF for these images was ≈1.″2. These observations consisted of four dithered sets of 10 co-added images of 30 s duration each in the *J* and *H* bands, and of four dithered sets of 20 co-added images of 15 s duration each in the *K* band. For each band, a set of identical integrations located ∼10′ off-source were obtained in order to determine the sky and telescope backgrounds. Both the on-source and off-source observations were dithered by ∼30″ in order to eliminate the effects of defective pixels. For both the 1994 November 22 and 1996 January 8 observations, the final image processing, consisting of background subtraction and field flattening obtained from differential dome flats, was accomplished by the SQIID suite of software operating within the IRAF environment.

[4] The Very Large Array is an instrument of the National Radio Astronomy Observatory (NRAO), which is operated by Associated Universities, Inc., under contract with the National Science Foundation.

Most of the known compact centimeter-wavelength sources in Orion (e.g., Felli et al. 1993; Churchwell et al. 1987; Garay, Moran, & Reid 1987) are associated with infrared point sources (e.g., McCaughrean & Stauffer 1994). A comparison between the VLA radio positions and the IRCAM infrared positions of 22 radio/near-infrared sources allowed a determination of the plate scale (0.″528 pixel^{-1}) and rotation (1.°22) of the IRCAM frames. Since the infrared and radio emission from the BN object are spatially coincident (Menten & Reid 1995), the IRCAM frames were placed into the VLA B1950 reference frame by aligning the IRCAM position of the BN object with the BN radio position as reported by Felli et al. (1993). As a check on the absolute astrometry of the IRCAM frames, the VLA positions of the 22 radio/near-infrared sources were then differenced with the IRCAM positions. It was found that the average difference and standard deviation between the VLA and IRCAM coordinates (VLA-IRCAM) was ΔR.A. $= 0.''06$, $\sigma = 0.''15$, Δdecl. $= -0.''06$, $\sigma = 0.''13$.

The IRCAM observations on 1996 January 8 were obtained on a night when all-sky photometry was carried out by observations of 10 standard stars from Elias et al. (1982) and Carter & Meadows (1995). Observations of the standard stars allowed the *J*-, *H*-, and *K*-band measurements of the infrared point sources to be placed on the standard magnitude and color system via determination of the nightly extinction coefficients and instrumental color terms. For comparison with sources A, B, and C in the Orion S region (see § 3), photometry was also obtained for 20 other point sources in the Orion S region. The 20 compact sources were selected on the basis of not saturating the detector at any wavelength and, at the same time, on the basis of having a good signal-to-noise ratio in spite of the bright and variable Orion cloud infrared nebulosity at the *J*, *H*, and *K* bands.

3. RESULTS

Figure 1 (Plate 46) shows an annotated gray-scale 2.2 μm image of Orion. Both the BN/KL and Orion S regions are shown (and annotated) in Figure 1, along with the Trapezium region. IRc2 is not detected in our images, but its location is marked in the figure. Although individual contour plots of the 2.2 μm emission toward the BN/KL and Orion S regions are shown in subsequent figures, Figure 1 provides an overall view of the 2.2 μm sources toward Orion, showing the spatial relationship between the BN/KL, Trapezium, and Orion S regions of the Orion Nebula. The coordinates of the near-infrared images have been placed into the radio frame (B1950) with an accuracy better than $\pm 0.''2$. Most of the 49 compact centimeter-wavelength radio sources in Orion cataloged by Felli et al. (1993) are associated with the near-infrared point sources seen in Figure 1 (also see McCaughrean & Stauffer 1994 and references therein). Menten & Reid (1995) have reported the detection of several additional compact radio sources, some of which are also associated with compact infrared components.

Figure 2 shows the spatial distribution of the water masers (shown as crosses) in the BN/KL region overlaid on contours of the 2.2 μm near-infrared emission. Several of the near-infrared components are annotated: IRc3, IRc4, IRc7, and BN. Other annotated components, g, n, and t, were cataloged by Lonsdale et al. (1982). The positions, velocities, and flux densities (corrected for primary beam attenuation)

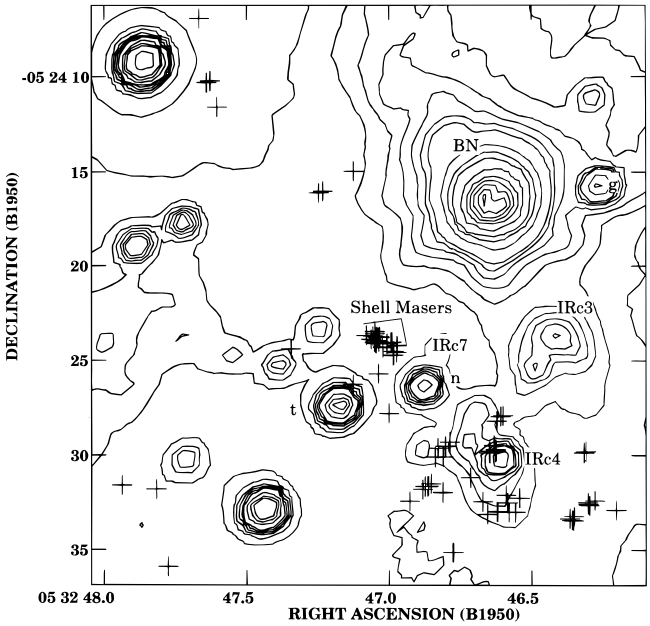

FIG. 2.—Overlay of the 2.2 μm IRCAM image of the BN/KL region (*contours*) with the positions of the BN/KL H_2O masers (*crosses*). Within the limitations of our experiment (see text), the spatial distribution of the water masers is consistent with that reported by Genzel et al. (1981). One clear exception is the region of "shell" H_2O masers, near IRc2. These were not observed with the VLBI baselines used by Genzel et al. (1981) but were easily imaged with the shorter baselines available with the VLA. The sizes of these features range from 50 to 80 mas.

of the detected H_2O masers in the BN/KL region are reported in Table 1. Because of primary beam attenuation by individual VLA antennas and the restricted velocity range (see § 2.1), it is likely that we have not reported a complete sample of all the masers in the BN/KL region. However, within these limitations, the general distribution of the masers shown in Figure 2 matches that of Genzel et al. (1981).

Genzel et al. (1981) did not detect the "shell" masers toward the IRc2 region. These were reported as being resolved on the long VLBI baselines. However, with the comparatively shorter baselines of the VLA, we have easily detected the shell masers. The Gaussian-fitted and beam-deconvolved sizes of the shell H_2O masers range from 50 to 80 mas (24–38 AU), somewhat smaller than the synthesized beam (see § 2.1). The question arises as to whether the sizes we measure for the shell masers represent the true sizes of the maser spots or whether these features are merely clusters of more compact masers, spatially blended in our 0.″1 beam. In the latter case, spatially blended features, the more compact masers would have been detected, and resolved into individual maser spots with the VLBI experiment of Genzel et al. (1981). The fact that Genzel et al. (1981) did not detect any of the shell masers using VLBI baselines indicates that the sizes we have measured for the shell masers are approximately the true sizes of the individual masers. Similar Gaussian fits made to other H_2O masers in the BN/KL and Orion S regions show that these maser features are unresolved, with sizes less than 0.″025. The location of the shell masers with respect to the other masers within the BN/KL region is shown in Figure 2. The shell masers are footnoted in Table 1.

Figure 3 is an expanded plot of the positions of the shell water masers. The masers are distributed in a $2'' \times 0.''5$ strip,

TABLE 1

H_2O Masers in Orion BN/KL

Radial Velocity (km s^{-1})	R.A. (B1950) (5 32)	Decl. (B1950) (−05 24)	Total Flux Density (Jy)
39.2	47.775	35.88	1.5
32.7	46.649	29.85	14.9
31.3	47.817	31.77	1.5
31.3	46.648	29.85	4.4
31.3	46.204	32.86	0.9
30.0	46.646	29.78	0.9
30.0	46.204	32.86	2.3
28.7	46.205	32.87	3.5
27.4	46.205	32.86	3.4
27.4	46.873	31.61	9.1
27.4	46.352	33.20	3.6
27.4	46.359	33.39	9.4
26.1	46.874	31.62	3.0
26.1	46.882	31.77	12.9
26.1	46.352	33.20	35.2
26.1	46.358	33.39	5.6
24.8	46.882	31.77	92.6
24.8	46.927	32.40	25.1
24.8	46.352	33.20	20.8
23.4	46.927	32.40	25.6
23.4	46.882	31.77	12.5
23.4	46.862	31.59	4.6
23.4	46.621	32.95	1.9
23.4	46.590	32.07	4.4
23.4	46.367	33.31	2.6
22.1	46.865	31.61	1.5
22.1	46.589	32.07	29.5
22.1	46.621	32.94	9.1
22.1	46.367	33.30	6.5
22.1	46.632	29.47	1.3
22.1	46.204	32.87	1.1
20.8	46.864	31.62	3.6
20.8	46.632	29.47	7.8
20.8	46.621	32.94	121.6
19.5	46.632	29.49	38.6
19.5	46.621	32.94	163.3
19.5	46.299	32.61	10.7
18.2	46.303	32.55	96.7
18.2	46.618	32.96	4.1
18.2	46.671	32.41	3.7
18.2	46.631	29.49	25.7
18.2[a]	46.984	24.50	21.6
18.2	47.937	31.55	22.8
18.2[a]	47.057	23.69	15.1
18.2[a]	47.051	23.57	26.8
16.9	47.937	31.55	284.5
16.9	46.303	32.56	1441.4
15.5	46.279	32.36	556.9
15.5	46.303	32.54	366.3
15.5	46.655	33.09	43.6
15.5[a]	47.052	23.44	61.7
15.5	47.937	31.55	693.4
14.2	47.937	31.56	1660.0
14.2	46.279	32.36	212.3
14.2	46.304	32.46	44.3
14.2	46.655	33.08	49.6
14.2[a]	46.994	24.02	70.9
14.2[a]	47.008	24.09	255.6
14.2[a]	47.051	23.45	59.5
14.2[a]	47.035	23.72	129.1
14.2[a]	47.043	23.72	29.0
12.9	47.938	31.56	1274.4
12.9	46.776	35.11	28.4
12.9[a]	46.991	24.01	96.0
12.9[a]	47.008	24.11	165.4
12.9	47.641	10.31	350.4
11.6	46.542	32.22	757.2
11.6	46.775	35.12	184.7
11.6	47.628	10.22	492.3
11.6	47.641	10.32	161.7
10.3	46.543	32.22	1687.1
10.3	47.629	10.23	583.0
9.0	47.001	27.81	182.1
9.0	46.810	30.07	70.6
9.0	46.853	31.48	474.7

TABLE 1—*Continued*

Radial Velocity (km s^{-1})	R.A. (B1950) (5 32)	Decl. (B1950) (−05 24)	Total Flux Density (Jy)
9.0	46.811	31.95	193.6
9.0	46.774	35.12	115.5
9.0	46.646	29.87	788.0
9.0	46.626	29.68	97.1
9.0	46.544	32.22	2022.3
9.0	46.354	33.42	369.9
7.6	46.853	31.47	897.7
7.6	46.646	29.87	13920.0
6.3	46.646	29.87	385.2
6.3	46.584	32.47	64.8
6.3	46.579	32.98	686.5
6.3	46.557	32.98	415.2
6.3	46.812	31.93	34.9
6.3	46.852	31.47	21.0
6.3	47.125	14.96	61.9
6.3	47.604	11.59	58.9
5.0	47.125	14.96	77.8
5.0	46.812	31.91	21.8
5.0	46.579	32.98	83.9
5.0	46.557	32.97	209.6
3.7	47.345	24.38	28.8
3.7	47.038	25.70	68.8
3.7	46.803	29.52	148.7
3.7	46.787	29.30	32.4
3.7	46.628	29.82	93.2
3.7	46.714	31.15	29.0
2.4	46.803	29.53	2333.4
2.4	46.625	29.76	39.1
1.0	46.802	29.53	986.6
1.0[a]	46.987	24.72	55.3
1.0	46.829	29.62	33.0
−0.3[a]	47.080	23.65	5.4
−0.3[a]	46.972	24.21	23.5
−0.3	46.829	29.62	7.3
−0.3	46.626	29.80	3.0
−0.3	46.621	28.19	3.3
−0.3	46.601	27.92	11.4
−0.3	46.609	27.96	14.9
−0.3[a]	46.974	24.56	70.7
−0.3[a]	46.984	24.70	32.9
−1.6	46.622	28.19	61.2
−1.6	46.838	30.08	144.2
−1.6[a]	46.973	24.20	19.7
−1.6[a]	47.022	24.31	14.6
−1.6[a]	47.052	24.01	4.3
−1.6[a]	47.046	24.09	13.1
−1.6	47.667	6.91	8.7
−2.9	47.233	16.01	49.8
−2.9	46.623	28.21	5.2
−2.9	46.838	30.09	32.4
−2.9[a]	47.034	23.76	12.8
−2.9[a]	47.022	24.28	20.1
−2.9[a]	47.047	24.07	131.0
−2.9[a]	47.052	23.99	82.6
−4.2	47.233	16.02	170.0
−4.2[a]	47.038	23.78	60.3
−4.2[a]	47.048	24.05	1013.1
−5.5	47.127	26.26	7.7
−5.5[a]	47.037	23.69	21.2
−5.5	47.233	16.03	54.9
−5.5	47.248	16.11	142.0
−5.5[a]	47.047	24.02	161.3
−5.5[a]	47.045	23.91	134.2
−6.9[a]	47.048	23.74	9.4
−6.9[a]	47.064	23.87	34.4
−6.9[a]	47.045	23.93	32.9
−6.9	46.318	29.87	30.4
−8.2[a]	47.064	23.86	60.4
−8.2	46.312	29.80	27.2
−8.2	46.317	29.85	16.7
−9.5	46.312	29.79	28.5

Note.—Units of right ascension are hours, minutes, and seconds, and units of declination are degrees, arcminutes, and arcseconds.

[a] Orion BN/KL shell maser (see text).

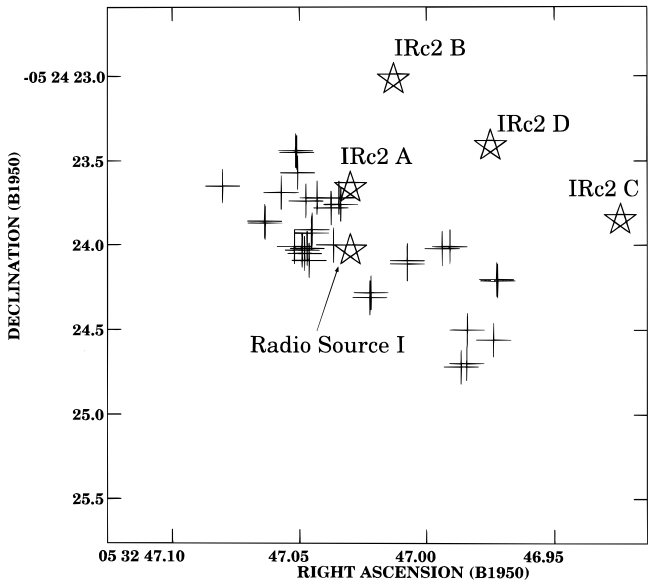

FIG. 3.—Overlay of the positions of the shell H_2O masers (*crosses*) with the positions of radio source I (Churchwell et al. 1987) and the four components of IRc2 (Dougados et al. 1993). Errors in the absolute positions of the water masers, radio source I, and the infrared components are estimated to be 0.″1, 0.″1, and 0.″2, respectively. The H_2O masers are found in a $2'' \times 0.''5$ strip, centered on radio source I. The H_2O masers do not appear to be directly associated with the components of IRc2.

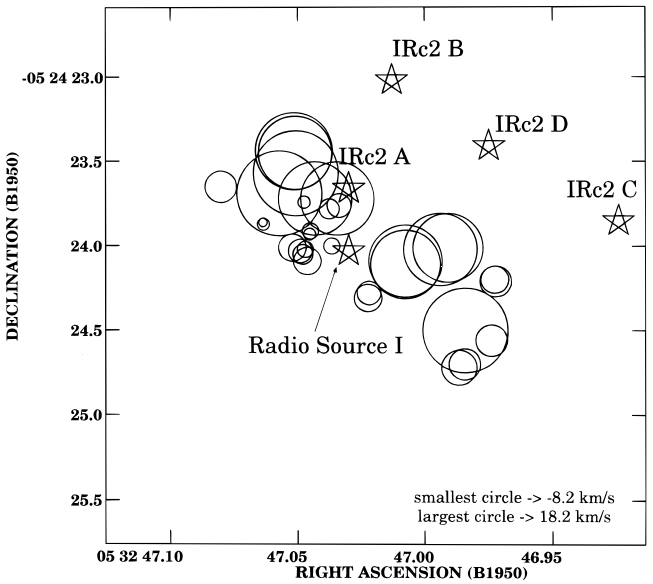

FIG. 4.—Overlay of the positions and velocities of the shell H_2O masers (*circles*) with the positions of radio source I (Churchwell et al. 1987) and the four components of IRc2 (Dougados et al. 1993). The circle centers mark the positions of individual maser features; the radius of the circle is proportional to the velocity of the maser feature. The smallest and largest circles correspond to velocities of -8.2 and 18.2 km s^{-1}, respectively.

with the major axis oriented NE-SW. The positions of radio source I (Churchwell et al. 1987) and the four components of IRc2 (Dougados et al. 1993) are overlaid on the maser positions. Although previously believed to be associated with IRc2 (see Genzel & Stutzki 1989 and references therein), it is now clear that the shell masers are *not* coincident with the components of IRc2 but are instead centered on radio source I. As can be seen from Table 1, the shell masers are clustered into two LSR velocity ranges: $-8.2 \rightarrow 1.0$ km s^{-1} and $12.9 \rightarrow 18.2$ km s^{-1}. Figure 4 is similar to Figure 3, except that the maser positions are marked by circles instead of crosses, with the velocity of individual maser features proportional to the radius of each circle. The velocity pattern of these masers, and the relationship between the H_2O masers and other molecular species, will be discussed in § 4.1. We note that the positions of the shell maser features within the BN/KL region have been illustrated by previous authors (e.g., Fig. 7 of Wright et al. 1990 or Fig. 10 of Genzel & Stutzki 1989). The overall distribution and detailed positions reported herein show general agreement with the illustrated positions of previous authors. A spectrum of all the masers detected in the BN/KL region is shown in Figure 5*a*; a spectrum of only the shell masers is found in Figure 5*b*.

The next several figures show our H_2O maser and near-infrared data for the Orion S region. The crosses in Figure 6 indicate the positions of the H_2O masers in the Orion S region, overlaid on contours of the near-infrared emission. The masers toward Orion S are found in a $15'' \times 20''$ region. Three very red pointlike infrared components are found near the masers. We call these components A, B, and C and have labeled them in Figure 6 accordingly, along with the positions and sizes of components CS 3 (Mundy et al. 1986) and FIR 4 (Mezger, Zylka, & Wink 1990). The maser group that we associate with the Orion S outflow is marked in Figure 6 by an arrow. The positions, velocities, and flux densities of the H_2O maser features in the Orion S region are listed in Table 2. Maser features associated with the Orion S outflow are footnoted in Table 2. A combined spectrum of all the masers in the Orion S region is shown in Figure 5*c*.

An expanded plot of the positions of the masers associated with the Orion S molecular outflow is shown in Figure 7. These masers are distributed in a thin 0.″6 strip, oriented NW-SE. A spectrum of these maser features is shown in Figure 5*d*. Figure 8 is similar to Figure 7, except that the positions of the masers are marked by circles instead of crosses, with the velocity of individual maser features proportional to the radius of each circle. The smallest circle corresponds to an LSR velocity of -20 km s^{-1}, the largest circle to a velocity of 44.5 km s^{-1}. The velocity pattern of these masers, and the relationship between the H_2O masers and other molecular species, will be discussed in § 4.2.

The three very red, compact near-infrared sources A, B, and C are located about 10″ north of the position of the CS 3 and FIR 4 millimeter-wavelength continuum components, and at the northern edge of the region of H_2O maser emission. In the following discussion, we assume that each of these sources are individual young stellar objects. Several maser features are found 0.″7 NE of near-infrared component C (see Fig. 6 and Table 2). The masers near component C are found in a velocity range of $-13.4 \rightarrow -6.9$ km s^{-1} and reach a peak flux density of 17 Jy in the -12.1 km s^{-1} channel. Because of the proximity to the Orion S molecular outflow, H_2O masers, and millimeter continuum sources, and our interest in whether or not any of the compact IR objects A, B, or C are the energy source for the Orion S region, we have performed photometry on the infrared data. The near-infrared *J*-, *H*-, and *K*-band magnitudes of A, B, and C are listed in Table 3. Figure 9 is a near-infrared color-color diagram of components A, B, and C along with 20 additional compact sources in the Orion S

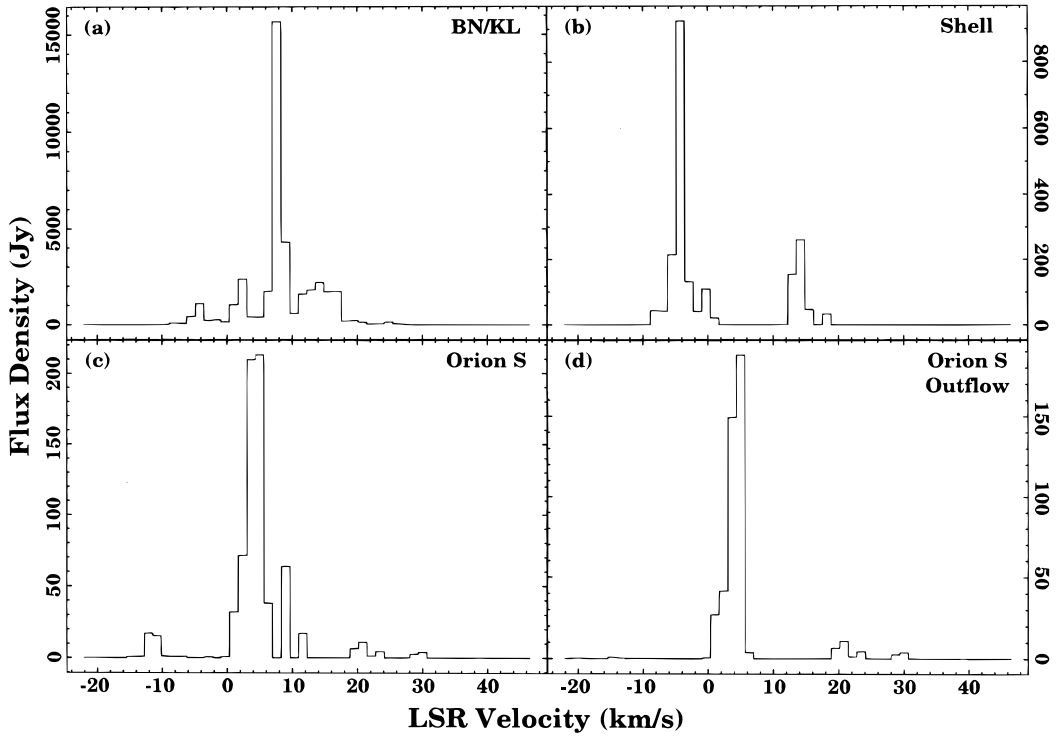

FIG. 5.—(*a*) Spectrum of the H_2O masers in the BN/KL region detected by our experiment. Maser features are found in a velocity range of -9.5–39.2 km s^{-1}. (*b*) Spectrum of the BN/KL H_2O masers found toward radio source I. Maser features are found in a velocity range of -8.2–18.2 km s^{-1}. (*c*) Spectrum of the H_2O masers found in the Orion S region. (*d*) Spectrum of the Orion S H_2O masers found toward the outflow region.

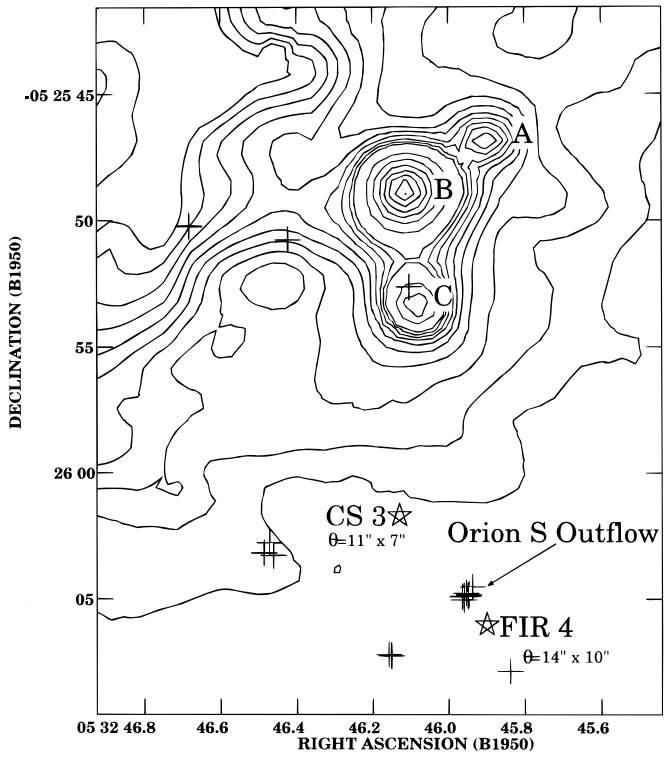

FIG. 6.—Overlay of the 2.2 μm IRCAM image of the Orion S region (*contours*) with the positions of the water masers (*crosses*). Near-infrared components A, B, and C are annotated, and the positions and sizes of continuum components CS 3 (Mundy et al. 1986) and FIR 4 (Mezger et al. 1990) are shown. The H_2O maser cluster associated with the Orion S molecular outflow is marked with an arrow.

region. In this figure, the solid curve represents the locus of main-sequence star colors, and the area between the dashed lines represents a region occupied by stars reddened by ordinary interstellar extinction. Stars lying to the right of the dashed region show an infrared excess, typically interpreted as emission from a hot circumstellar dust shell. It is clear that components A, B, and C are very red. Component A lies well to the right of the dashed lines, with a significant infrared excess, and appears slightly extended with respect to the 1.″2 PSF, along an E-W position angle (the E-W extension can be seen in the *K*-band images [see Fig. 6] but is more easily seen in the *J*- and *K*-band images, which are not shown here). Component C is deeply embedded, may show evidence of modest infrared excess, and appears as a point source in our images. Component B is probably the most interesting of the three since its position in the two-color diagram implies that it is the most deeply embedded component and that it is without circumstellar dust emission. This, in conjunction with component B's apparent *K* magnitude, implies that it is the most luminous of the three sources. In the *K*-band image, component B may be slightly extended with respect to the PSF, although with circular symmetry. The *H*-band image shows some asymmetries in this component, with a "tongue" of extended emission extending slightly to the south. It is difficult, however, to determine if this extended emission is truly associated with component B or merely a chance superposition, since components A, B, and C are embedded (or projected) in a region of extended emission with considerable small-scale structure. Using our *J*-, *H*-, and *K*-band calibrated images, we take 2.4 mag for the $H-K$ color of component B and find

TABLE 2

H_2O MASERS IN ORION S

Radial Velocity (km s^{-1})	R.A. (B1950) (5 32)	Decl. (B1950) (−05)	Total Flux Density (Jy)
44.5[a]	45.938	26 04.52	0.2
39.2[a]	45.947	26 04.82	0.2
30.0[a]	45.951	26 04.87	4.0
28.7[a]	45.951	26 04.87	2.7
23.4[a]	45.949	26 04.89	4.6
22.1[a]	45.949	26 04.88	1.3
20.8[a]	45.955	26 04.76	11.0
19.5[a]	45.955	26 04.76	6.6
11.6	46.462	26 03.29	17.2
9.0	46.472	26 02.79	23.3
9.0	46.683	25 05.25	40.4
6.3	46.487	26 03.19	11.8
6.3[a]	45.960	26 04.88	3.9
6.3	45.839	26 07.84	22.4
5.0	46.158	26 07.18	25.1
5.0[a]	45.961	26 04.88	187.9
3.7[a]	45.961	26 04.88	149.3
3.7	46.158	26 07.18	39.7
3.7	46.152	26 07.23	20.6
2.4	46.151	26 07.24	29.6
2.4[a]	45.961	26 04.88	41.5
1.0[a]	45.961	26 04.88	27.1
1.0	46.151	26 07.23	4.9
−0.3[a]	45.961	26 04.88	0.5
−0.3	46.424	25 50.76	0.3
−2.9	46.684	25 50.21	0.7
−6.9	46.104	25 52.62	1.0
−8.2	46.104	25 52.62	0.7
−9.5	46.105	25 52.61	1.1
−9.5[a]	45.965	26 04.90	0.1
−10.8	46.105	25 52.60	15.4
−12.1	46.105	25 52.60	17.2
−13.4	46.105	25 52.61	0.5
−13.4[a]	45.960	26 05.03	0.4
−14.8[a]	45.960	26 05.03	0.8
−20.0[a]	45.960	26 05.03	0.2

NOTE.—Units of right ascension are hours, minutes, and seconds, and units of declination are degrees, arcminutes, and arcseconds.

[a] Orion S outflow maser (see text).

an extinction of 3.6 mag at K. Correcting for this extinction gives an apparent magnitude of 6.8. If this object is at a distance of 500 pc, the absolute magnitude is −1.7. If object B is a zero-age main-sequence (ZAMS) star, this would be a B2 star (see, e.g., Megeath 1994, Fig. 4). From Panagia (1973), this star has a luminosity of 2900 $L_\odot$, more than 30% of the luminosity estimated for the Orion S region (Drapatz et al. 1983). A similar analysis shows that object C exhibits colors that are consistent with those expected for a ZAMS A0 star. The infrared colors of component A are heavily contaminated by circumstellar dust emission, which prevents a determination of a spectral type for this component.

It appears unlikely that infrared component B is the energy source for the Orion S region. Although B could contribute to the heating of the northern portion of the Orion S dust cloud, at a projected separation of ≈15″ it is

TABLE 3

INFRARED MAGNITUDES OF OBJECTS A, B, AND C

Object	J	H	K
A	13.89 (0.07)	12.92 (0.05)	11.99 (0.05)
B	>17.00	12.69 (0.05)	10.32 (0.05)
C	15.00 (0.08)	12.61 (0.05)	11.18 (0.05)

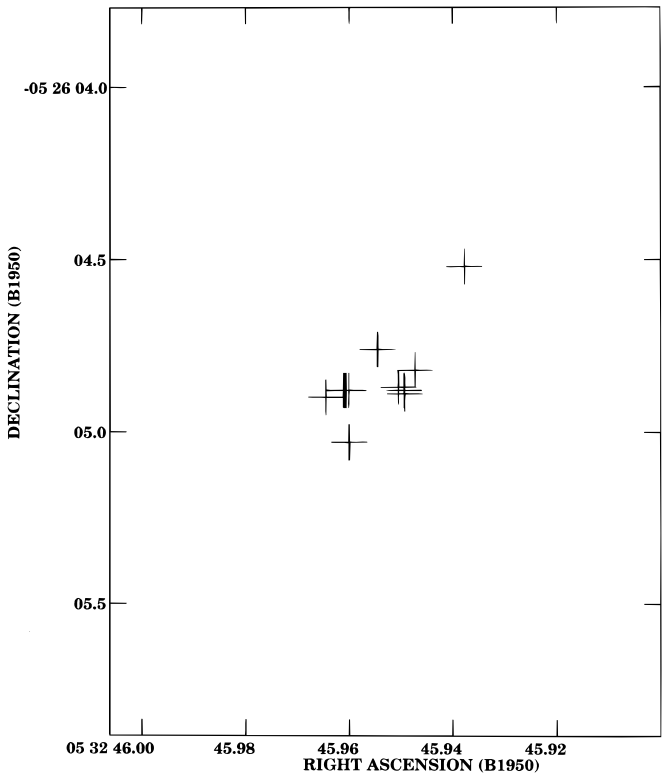

FIG. 7.—Expanded plot of the H_2O maser cluster associated with the Orion S outflow. The masers are found in a thin strip, oriented NW-SE.

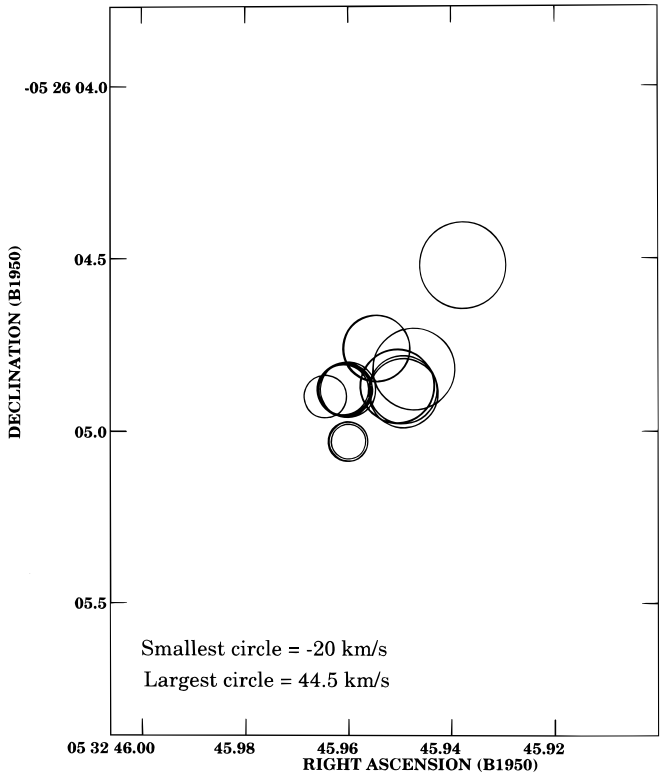

FIG. 8.—Similar to Fig. 7, except that the positions of the maser features are indicated by circles whose radii are proportional to the velocity of the maser feature. The smallest and largest circles correspond to velocities of −20 and 44.5 km s^{-1}, respectively.

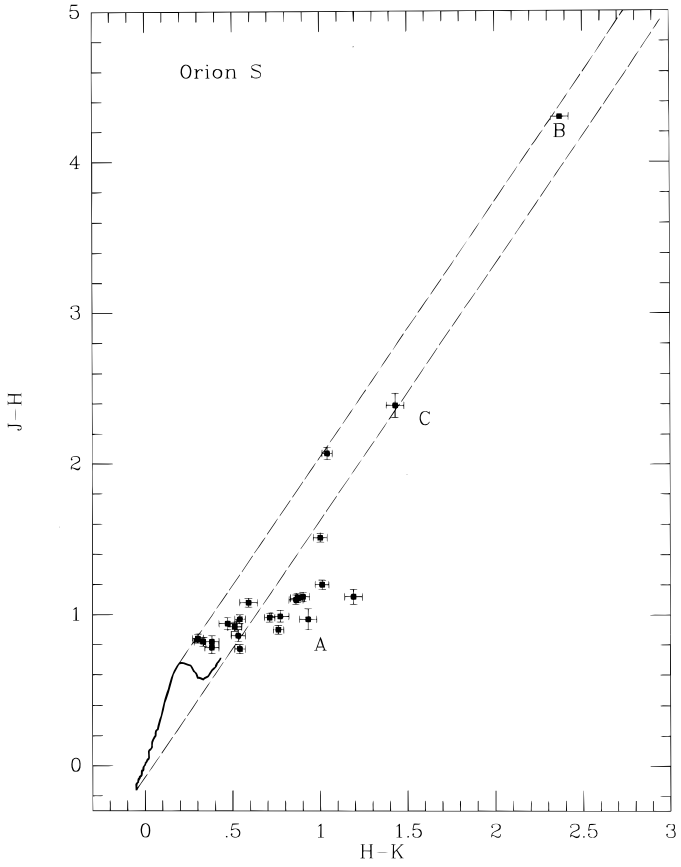

FIG. 9.—Near-infrared color-color diagram of several (20) compact sources near the Orion S region, showing the location of A, B, and C. The solid curve represents the locus of main-sequence star colors, and the area between the dashed lines represents a region occupied by stars reddened by ordinary interstellar extinction. Stars lying to the right of the dashed lines are likely surrounded by hot circumstellar dust shells.

too distant to be the sole energy source. More likely, the energy source of the Orion S outflow is deeply embedded within the core of the dust cloud, completely extincted in the infrared K band. As with the shell masers in the BN/KL region, the Orion S water masers are not associated with a near-IR source. These are two examples that show that the association of H_2O masers with near-IR objects can easily lead to incorrect conclusions.

There are no CH_3OH or OH masers in the Orion S region. This is in marked contrast to the Orion BN/KL region where the $J_2 \rightarrow J_1$ lines of CH_3OH (Johnston et al. 1992, 1997) and OH masers (Johnston et al. 1989) are prominent. This difference could be caused by excitation effects, presumably related to the interaction of the outflow with nearby dense quiescent gas, or by lower abundances of CH_3OH and OH in the Orion S region.

4. DISCUSSION

4.1. *Shell* H_2O *Masers*

There has been much discussion regarding the origin of the energetic phenomena observed in the Orion BN/KL region. IRc2 has often been suggested as the location of the central energy source. However, it is becoming increasingly clear that IRc2 is near to, but not coincident with, the central energy source of the BN/KL region. It has been known for some time (see, e.g., Wright et al. 1990) that the compact SiO masers are found to the south of IRc2. Menten & Reid (1995) have demonstrated convincingly that the SiO masers are instead coincident with radio component I (Churchwell et al. 1987). We have shown (see Fig. 3) that, like the SiO masers, the shell H_2O maser distribution is centered on radio component I rather than on IRc2.

It is interesting to compare the spatial distribution of the shell H_2O masers with that of the SiO masers. Whereas the intense SiO masers are distributed in a region of diameter 0.″2, or $\approx$80 AU (see, e.g., Plambeck, Wright, & Carlstrom 1990), the shell H_2O masers are found in a larger elliptical region, $2'' \times 0.''5$ ($\approx 1000 \times 250$ AU), with the major axis oriented NE-SW (roughly perpendicular to the larger molecular outflow). Although the distribution of the intense SiO masers is considerably more compact than that of the H_2O masers, recent observations of the $v = 0$, $J = 1$–0 (Chandler & De Pree 1995) and $v = 0$, $J = 2$–1 (Wright et al. 1995) transitions of SiO show a more extended distribution. The size and orientation of this elliptical or disklike SiO structure is quite similar in size to that of the H_2O masers. This suggests a direct kinematic relation between the extended SiO emission and the H_2O maser cloud.

The velocity distribution of the intense SiO masers has been explained by a combination of Keplerian rotation and outflow (Plambeck et al. 1990). For the H_2O masers, the most blueshifted masers are found directly to the east of radio component I. Redshifted masers are found projected near the blueshifted masers, and also to the SW of radio component I. There appears to be no simple model for the velocity pattern of the shell H_2O masers (Fig. 4). Wright et al. (1995) found that the rotation and outflow model for the inner (80 AU) SiO masers cannot be easily extended to the 1000 AU SiO disk. It is likely that the velocity field of the molecular gas surrounding radio component I becomes significantly less ordered farther away from radio component I.

4.2. *Orion S Region*

H_2O masers in the Orion S region are found in a $15'' \times 20''$ region. One maser cluster is projected near the infrared component C, possibly a ZAMS A0 star. However, the most interesting cluster of H_2O masers is found near R.A. = $05^h32^m45^s.95$, decl. = $-05°26'4''.75$. At this location, we find a group of intense masers distributed in a thin strip or disklike structure of length $\approx$0.″6. (Fig. 7). These masers cover a 65 km s^{-1} range, with the most blueshifted masers found at the SE end of the disklike distribution and the most redshifted masers found at the NW end (Fig. 8).

Tartar & Welch (1986) had proposed that H_2O masers are formed behind shocks resulting from the interaction of outflows with quiescent clouds. Thus, the positions of H_2O masers need not coincide with the position of the outflow source itself. However, in the case of Orion S, the H_2O masers cover a radial velocity range of 65 km s^{-1} in a very small region. This large range in radial velocity is in contrast to the rather small range of radial velocity found for the highly collimated Orion S outflow (Schmid-Burgk et al. 1990). We believe that the large velocity spread in H_2O maser velocities is caused by motions close to the outflow source, and thus we propose that the large range of H_2O maser velocities at the maser center is the signature of the outflow source. Although this H_2O maser center is $\approx 4''$ from the continuum center given by McMullin et al. (1993), the dust emission is extended over about 10″. Quasi-thermal

SiO and H_2O masers are SW of the dust continuum maximum. We note that, like the Orion BN/KL shell masers discussed in the previous section, the Orion S outflow masers have a thin disklike distribution. As discussed previously, the long axis of the BN/KL shell H_2O masers' distribution is roughly perpendicular to the axis of the BN/KL outflow. Similarly, the long axis of the disklike distribution of the Orion S outflow H_2O masers is approximately perpendicular to the highly collimated CO outflow (Schmid-Burgk et al. 1990).

There must be a direct relation between the high-excitation molecular region (traced by H_2O masers) and the outflow. Presumably there is a young star in the emission-line region that gives rise to the CO outflow. The new H_2O maser results show that there is a large concentration of maser centers near the dust continuum peak found by McMullin et al. (1993). The conversion of dust continuum intensity to mass is uncertain by a factor of up to 10 (see, e.g., Gordon 1995). According to McMullen et al. (1993) and Mezger et al. (1990), the most reasonable estimate for the mass of the compact source in Orion S from the dust data is $\approx 50\ M_\odot$. This estimate is approximately 50% of the mass estimated for the Orion hot core source. With such a small difference in mass, it is surprising that Orion S does *not* show the richness of molecular emission found in the Orion hot core. Although McMullin et al. (1993) have found emission from SiO, $H^{13}CO^+$, SO_2, CH_3OH, and HC_3N within 10″ of our H_2O maser position, this emission is relatively weak. McMullin et al. (1993) interpreted the differences in abundance between Orion S and Orion KL as being the result of age. In their view, the chemical evolution of Orion S is less advanced than in Orion KL. Since kinematic evidence indicates that the outflow in Orion KL is less than 10^4 years old, the Orion S source must be even younger. On this basis, Orion S would be one of the youngest stars in the Galaxy.

The energetics of the collimated CO outflows depend on $\sec^3 i$, where i is the angle between the outflow direction and the line of sight (see, e.g., the discussion in Schmid-Burgk et al. 1990). Thus, it is possible that the energetics of the CO outflows are even more uncertain than the masses of the Orion hot core and Orion S, because of geometry. The Orion KL outflow, 6″ N of the hot core (see, e.g., Wilson, Serabyn, & Henkel 1986), reaches high radial velocities and is spatially very compact. This indicates an outflow close to the line of sight, i.e., i close to 0°. In contrast, the Orion S outflow exhibits a much lower radial velocity and a larger angular size. This indicates a direction perpendicular to the line of sight, i.e., i close to 90°. Given these uncertainties, any discussion of energetics that is based on properties of the collimated CO outflows will be inconclusive. An alternative would be to use the FWZP of the more poorly collimated quasi-thermal SiO emission. From the data of Ziurys et al. (1990), the Orion KL outflow has a FWZP line width that is 4 times that found for the Orion S outflow. Using the simplest relation between line width and energy, this indicates that the energy of the outflow from the Orion KL region is a factor of 16 larger than the outflow from Orion S. From measurements of far-IR flux densities, the total luminosity is $\approx 10^4\ L_\odot$ (Drapatz et al. 1983). The luminosity of Orion KL is a factor of 10 larger than Orion S (see, e.g., Genzel & Stutzki 1989). It is possible that the good agreement between luminosity and outflow energy is merely fortuitous, but taken at face value it would suggest that the conversion factor of luminosity to mechanical energy is the same for these two sources.

If the stellar luminosity of $10^4\ L_\odot$ (Drapatz et al. 1983) is caused by a single object, the exciting source is a star of type B0.5 (Panagia 1973). Presumably the surroundings are not ionized because the high gas density leads to rapid recombination. Perhaps more significant is the large amount of dust, which absorbs ionizing photons. Both of these effects would allow only a very small Strömgren sphere. There may be more than one star, but we conclude that the most massive star is associated with the centroid of the H_2O maser distribution, near $\alpha = 5^h32^m45^s.95$, $\delta = -05°26'04''.75$ (1950.0). This is presumably the source of the CO outflow.

The spatially extended surroundings of Orion S show an extraordinary set of conditions; it is useful to compare the properties of Orion KL with Orion S. Orion S shows 6 cm H_2CO absorption, which has a temperature lower than -4 K. The depth of the line absorption requires a background continuum source. An H_2CO multiline analysis shows that the H_2 density must be $\sim 10^4$ cm^{-3}. Since a compact continuum source is not detected with the VLA, the H_2CO must be absorbing an extended continuum region, perhaps a part of the Orion A H II region itself. This had been proposed by Johnston et al. (1983), and the newer H_2CO results of Mangum et al. (1993) and the continuum data of Felli et al. (1993) fully support this. The H_2CO absorption is offset 20″ NW of the CO outflow. There is little overlap of the high-velocity CO outflow and the H_2CO. However, there is a coincidence between the H_2CO region and one lobe of a second CO outflow that J. Schmid-Burgk (1997, private communication) has discovered in Orion S. The latter outflow shows extremely high velocities and is very compact. Since the compact outflow source and the H_2CO absorption region have nearly the same projected location, the simplest interpretation is that the outflow and H_2CO regions are related. From the H_2 density and kinetic temperature of the H_2CO region, the molecular gas has a lower pressure and is being compressed by the ionized gas. The H_2CO absorption cloud cannot lie entirely in front of the H II region, since the absorption cloud is not seen optically. On the other hand, the H_2CO absorption cloud cannot lie completely behind the H II region either, otherwise there would be no absorption. Therefore, we conclude that the H_2CO absorption cloud and, by association, the Orion S region are most likely part of a molecular protrusion into the H II region itself. For an 8000 K ionized gas, this is an emission measure of 2.6×10^4 cm^{-6} pc. If the electron density is $\approx 10^5$ cm^{-3}, a path length of 8×10^{12} cm is required. The extended region toward Orion KL and the hot core shows only H_2CO emission, indicating H_2 densities greater than 10^6 cm^{-3}. Although the two most prominent IR and submillimeter sources in the OMC cloud are separated by $\approx 100''$, they have very different physical conditions: (1) Orion KL is behind (but close to) the H II region, while Orion S is *inside* the H II region itself. Because of the high-H_2 density, molecular gas may have halted the expansion of Orion A, but this cannot be the case for Orion S; (2) the directions of the outflows are nearly at right angles on the sky (the Orion KL outflow is nearly NW-SE, while the Orion S outflow is nearly NE-SW) and also are 90° with respect to the line-of-sight direction. The Orion KL outflow is nearly along the line of sight, while the Orion S outflow is nearly perpendicular to the line of sight. This may indicate that the magnetic fields do not play an important role in the

evolution of these regions, and (3) Orion S appears to be younger, although the formation of complex molecules may be hindered because of the influence of the H II region.

5. SUMMARY

We have observed the 1.3 cm transition of H_2O in the Orion region of star formation and found maser emission in both the Orion BN/KL and Orion S regions. In addition, we have imaged the Orion region in the near-infrared, searching for the excitation source of the Orion S outflow. We did not detect CH_3OH or OH maser emission, or centimeter-wavelength continuum emission, from the Orion S region. The specific results and conclusions of this study are as follows:

1. We have found that the H_2O masers in Orion BN/KL are distributed in a $30'' \times 30''$ region. A subset of these masers, the "shell" water maser cluster, is distributed in a $2'' \times 0''.5$ strip oriented NE-SW and centered on radio component I rather than on any of the components of IRc2. The masers are slightly smaller (24–38 AU) than the synthesized beam, and their distribution is similar to the 1000 AU disk-like distribution of the $v = 0$, $J = 1$–0 and $v = 0$, $J = 2$–1 transitions of quasi-thermal SiO. The orientation of the major axis of the maser distribution is roughly perpendicular to the large-scale molecular outflow. The average spectrum of the shell H_2O masers is similar to that of the intense, compact (80 AU) SiO masers.

2. We have found H_2O masers in the Orion S region that are distributed in a $15'' \times 20''$ region. A subset of these masers is distributed in a narrow strip $0''.6$ in extent, near R.A. = $05^h32^m45^s.95$, decl. = $-05°26'4''.75$. The strip is oriented SE-NW, with the most blueshifted masers found at the SE end and the most redshifted masers toward the NW. The highly collimated CO outflow in Orion S is oriented approximately perpendicular to the major axis of the H_2O maser distribution. We propose that the excitation source of the Orion S outflow and the heating source of the dust emission are at the position of this H_2O maser cluster.

3. We have imaged the entire Orion BN/KL and S regions in the near-infrared. A search for infrared emission from the heating source of the Orion S dust cloud produced negative results. A cluster of three very red stellar sources was found just to the north of the Orion S region. One of these infrared components is likely a ZAMS star of spectral type B2. This component could contribute to the heating of the northern part of the Orion S dust cloud but is not the main energy source. Searches for CH_3OH and OH masers in Orion S produced negative results, as did a search for centimeter-wavelength continuum.

T. L. W. and K. J. J. were supported in part by the Max-Planck-Forschungspreis, administered by the A. von Humboldt–Stiftung. The authors thank S. Casement and H. Guetter for assistance with the IRCAM data, and T. Megeath and M. McCaughrean for useful discussions on the nature of the infrared components in the Orion S region.

REFERENCES

Batrla, W., Wilson, T. L., Ruf, K., & Bastien, P. 1983, A&A, 128, 279
Carter, B. S., & Meadows, V. S. 1995, MNRAS, 276, 734
Chandler, C. J., & De Pree, C. G. 1995, ApJ, 455, L67
Churchwell, E., Felli, M., & Wood, D. O. S., & Massi, M. 1987, ApJ, 321, 516
Dougados, C., Lena, P., Ridgway, S. T., Christou, J. C., & Probst, R. G. 1993, ApJ, 406
Drapatz, S., Haser, L., Hofmann, R., Oda, N., & Iyengar, K. V. K. 1983, A&A, 128, 207
Elias, J. H., Frogel, J. A. Matthews, K., & Neugebauer, G. 1982, AJ, 87, 1029
Felli, M., Churchwell, E. B., Wilson, T. L., & Taylor, G. B. 1993, A&AS, 98, 137
Garay, G., Moran, J. M., & Reid, M. J. 1987, ApJ, 314, 535
Genzel, R., Reid, M. J., Moran, J. M., & Downes, D. 1981, ApJ, 244, 884
Genzel, R., & Stutzki, J. 1989, ARA&A, 27, 41
Gordon, M. A. 1995, A&A, 301, 853
Johnston, K. J., Gaume, R. A., Stolovy, S., Wilson, T. L., Walmsley, C. M., & Menten, K. M. 1992, ApJ, 385, 232
Johnston, K. J., Gaume, R. A., Wilson, T. L., Nguyen, H. A., & Nedoluha, G. E. 1997, ApJ, 490, 758
Johnston, K. J., Migenes, V., & Norris, R. P. 1989, ApJ, 341, 847
Johnston, K. J., Palmer, P., Wilson, T. L., & Bieging, J. H. 1983, ApJ, 271, L89
Keene, J., Hildebrand, R. H., & Whitcomb, S. E. 1982, ApJ, 252, L11
Lonsdale, C. J., Becklin, E. E., Lee, T. J., & Stewart, J. M. 1982, AJ, 87, 1819
Mangum, J. G., Wootten, A., & Plambeck, R. L. 1993, ApJ, 409, 282
McCaughrean, M. J., & Stauffer, J. R. 1994, AJ, 108, 1382
McMullin, J. P., Mundy, L. G., & Blake, G. A. 1993, ApJ, 405, 599
Megeath, S. T. 1994, in The Structure and Content of Molecular Clouds, ed. T. L. Wilson & K. J. Johnston (New York: Springer), 215
Menten, K. M., & Reid, M. J. 1995, ApJ, 445, L157
Mezger, P. G., Zylka, R., & Wink, J. E. 1990, A&A, 228, 95
Mundy, L. G., Scoville, N. Z., Baath, L. B., Masson, C. R., & Woody, D. P. 1986, ApJ, 304, L51
Panagia, N. 1973, AJ, 78, 929
Plambeck, R. L., Wright, M. C. H., & Carlstrom, J. E. 1990, ApJ, 348, L65
Schmid-Burgk, J., Guesten, R., Mauersberger, R., Schulz, A., & Wilson, T. L. 1990, ApJ, 362, L25
Tartar, J. C., & Welch, W. J. 1986, ApJ, 305, 467
Wilson, T. L., Serabyn, E., & Henkel, C. 1986, A&A, 167, L17
Wright, M. C. H., Carlstrom, J. E., Plambeck, R. L., & Welch, W. J. 1990, AJ, 99, 1299
Wright, M. C. H., Plambeck, R. L., Mundy, L. G., & Looney, L. W. 1995, ApJ, 455, L185
Ziurys, L. M., Wilson, T. L., & Mauersberger, R. 1990, ApJ, 356, L25

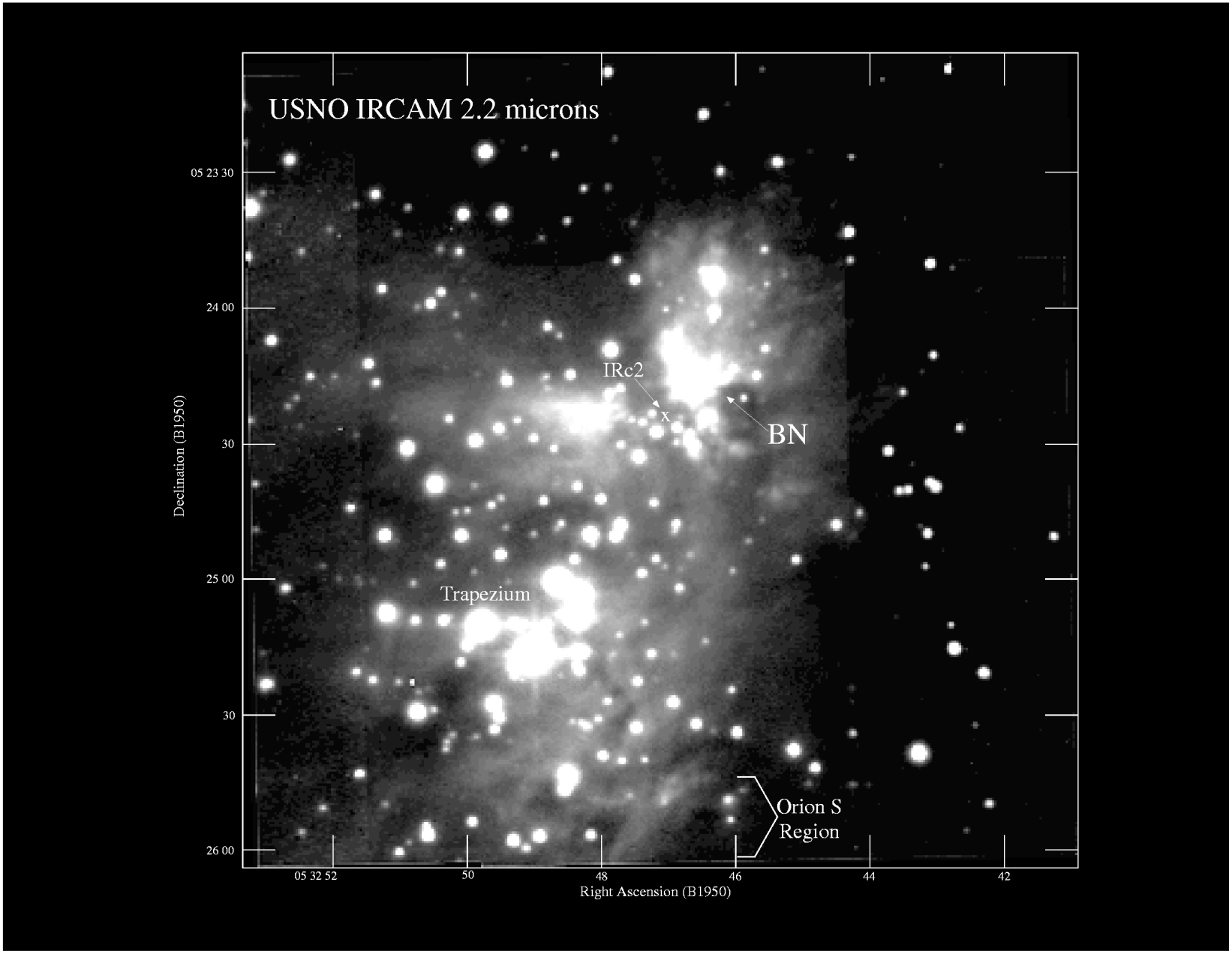

FIG. 1.—USNO IRCAM image of the Orion Nebula at a wavelength of 2.2 μm. This plot depicts the spatial relationship between the IRc2, BN/KL, Orion S, and Trapezium regions, which are annotated.

GAUME et al. (see 493, 942)